

Dielectric response with short-ranged electrostatics

Stephen J. Cox¹

Department of Chemistry, University of Cambridge, Lensfield Road, Cambridge CB2 1EW, United Kingdom^{a)}

(Dated: 5 August 2020)

The dielectric nature of polar liquids underpins much of their ability to act as useful solvents, but its description is complicated by the long-ranged nature of dipolar interactions. This is particularly pronounced under the periodic boundary conditions commonly used in molecular simulations. In this article, the dielectric properties of a water model whose intermolecular electrostatic interactions are entirely short-ranged are investigated. This is done within the framework of local molecular field theory (LMFT), which provides a well controlled mean-field treatment of long-ranged electrostatics. This short-ranged model gives a remarkably good performance on a number of counts, and its apparent shortcomings are readily accounted for. These results not only lend support to LMFT as an approach for understanding solvation behavior, but are relevant to those developing interaction potentials based on local descriptions of liquid structure.

I. INTRODUCTION

Understanding the dielectric nature of polar fluids is one of the principal aims of liquid state theory, and continues to be the motivation for both experimental^{1–3} and theoretical^{4–13} investigations. As can be immediately deduced from the fact that the free energy of a polar system depends on its shape,¹⁴ the dipolar interactions that define a polar fluid are long-ranged (LR). This makes their study both fascinating and complicated. The importance of understanding the dielectric properties of polar liquids cannot be overstated, as they play a crucial role in phenomena such as solvation, self-assembly, and transport through membranes and nanopores.^{15–18} Consequently, there are broad implications across the biological, chemical, physical and materials sciences. Of all polar liquids, water stands out owing to its ubiquity across disciplines. It is the focus of this article.

In addition to experiments, computer simulation is a widely taken approach to investigate the behavior of liquids at the molecular level. The computational cost associated with the microscopic resolution that simulations provide, however, often limits their application to system sizes far below that of samples investigated experimentally. As a result, periodic boundary conditions (PBC) are often employed to mitigate spuriously high degrees of interfacial curvature and surface-to-volume ratios. How to appropriately account for the LR nature of electrostatic interactions, and the implications this has for dielectric properties, has a long history.^{19–28} While certainly not the only method available to deal with electrostatic interactions under PBC, Ewald summation techniques are now widely considered the *de facto* standard.²⁹ On the one hand, it is hard to argue against the success that Ewald approaches have enjoyed as a computational tool. On the other, they are not especially intuitive, and risk masking simple physical interpretations of liquid state behavior.

In this article, the dielectric properties of liquid water whose intermolecular electrostatic interactions are entirely short-ranged (SR) will be investigated. Specifically, the framework provided by *local molecular field theory* (LMFT)^{30,31} will be exploited in order to recast LR electrostatic interactions in a mean-field, yet well controlled, fashion. Aside from demonstrating how LMFT’s performance can be understood within the existing statistical mechanical framework for polar liquids, the insight obtained from this study will aid the development of SR intermolecular potentials, which is often the case with modern machine-learning approaches.^{32–36} It will also help us to understand when neglect of LR electrostatics does, and does not, have severe consequences on simulated observables. Moreover, it seems likely that strong connections exist between LMFT ideas and classical density functional theory (see Refs. 37 and 38 for differing suggestions), and it is hoped that the results that follow will help the development of such theoretical approaches. The results presented here also provide further support to LMFT as a theoretical approach for understanding the solvation of charged species.^{38,39}

LMFT AND THE DIELECTRIC CONSTANT

LMFT is a statistical mechanical framework based on the Yvon-Born-Green hierarchy of equations that relate molecular correlations with intermolecular forces.³¹ The premise of LMFT is that the intermolecular interactions (or a subset) can be partitioned into SR and LR portions, and that there exists a mapping to a ‘mimic’ system. This mimic system comprises intermolecular interactions arising solely from the SR portion, and a suitably chosen one-body potential; by construction, the average structure and higher order correlations of the full system are captured. Although LMFT can be applied more generally,⁴⁰ only its application to electrostatic interactions is considered here. Moreover, as detailed derivations have been given elsewhere,³¹ discussion will be limited to its most salient features.

^{a)}Electronic mail: sjc236@cam.ac.uk

Let us begin by noting that the Coulomb potential can be separated exactly into SR and LR contributions,

$$\frac{1}{r} = \frac{\text{erfc}(\kappa r)}{r} + \frac{\text{erf}(\kappa r)}{r} \equiv v_0(r) + v_1(r), \quad (1)$$

where κ^{-1} defines the length scale over which v_0 decays. This will be familiar to many as the same procedure taken in Ewald approaches (see e.g. Ref. 28), where κ is chosen to optimize computational efficiency. In contrast, the success of LMFT relies on a choice of κ such that the mimic system accurately captures the one-body density and correlations of the full system. In what follows $\kappa^{-1} = 4.5 \text{ \AA}$, which has been previously demonstrated to be a reasonable choice.³¹ Instead of computing LR electrostatic interactions explicitly, the effects of v_1 are accounted for by a static restructuring potential,

$$\mathcal{V}_R(\mathbf{r}) = \mathcal{V}(\mathbf{r}) + \int d\mathbf{r}' n_R(\mathbf{r}') v_1(|\mathbf{r} - \mathbf{r}'|), \quad (2)$$

where n_R is the average charge density in the mimic system, \mathcal{V} is an external electrostatic potential that would be applied to the full system, and the integral is understood to be taken over all space. As \mathcal{V}_R is to be chosen such that $n_R = n$, where n is the average charge density of the full system, Eq. 2 defines a self-consistent relationship between \mathcal{V}_R and n_R . In a ‘pure’ LMFT approach, Eq. 2 can be solved either by brute-force or by exploiting linear-response theory.⁴¹ As the focus of this article is on understanding dielectric properties within the LMFT framework, here a more pragmatic approach is instead taken: The self-consistent cycle is ‘short-circuited’ by using n obtained from a simulation of the full system as the initial, and only, guess.⁴² While Eq. 2 has a simple mean-field form, it is important to stress that it is not derived from a mean-field ansatz. It represents a controlled approximation provided that the mimic system is chosen carefully. It should also be noted that Eq. 2 has been derived with non-uniform systems in mind, and that for uniform systems, more sophisticated LMFT approaches exist.^{42–44} When considering uniform systems in this study, however, the *strong-coupling approximation* (SCA) will be used, in which the integral in Eq. 2 is simply ignored i.e., $\mathcal{V}_R = \mathcal{V}$.

The central quantity describing the dielectric behavior of materials is the static dielectric constant ϵ . A natural question thus arises: Can we expect SCA to accurately capture ϵ of the full system? Following Madden and Kivelson,⁴⁵ it is taken as an empirical fact that ϵ is an intensive material property, and therefore does not depend on the shape of the sample under consideration. This provides the freedom to choose any geometry for which it is convenient to calculate ϵ , including an infinite system in which boundaries are not present. In this case, it is well established that

$$\frac{(2\epsilon + 1)(\epsilon - 1)}{9y\epsilon} = 1 + \frac{4\pi\rho}{3} \int_0^\infty dr r^2 h_\Delta(r), \quad (3)$$

with $y = 4\pi\beta\rho\mu^2/9$, where ρ is the number density, μ is the magnitude of the permanent molecular dipole moment, and $\beta = 1/k_B T$. (T is the temperature, and k_B is Boltzmann’s constant.) $h_\Delta = 3\langle h(1,2)\boldsymbol{\mu}_1 \cdot \boldsymbol{\mu}_2/\mu^2 \rangle_{\Omega_1\Omega_2}$ is the projection of the total correlation function $h(1,2)$ on to the rotational invariant $\boldsymbol{\mu}_1 \cdot \boldsymbol{\mu}_2/\mu^2$, where $\boldsymbol{\mu}_i$ is the dipole vector of molecule i , and $\langle \dots \rangle_{\Omega_1\Omega_2}$ denotes an unweighted average over the orientations of molecules 1 and 2. Crucial to the current study is that, for an infinite system, $h_\Delta \sim 0$ beyond some microscopic distance ℓ_ϵ .⁴⁶ Hence, ϵ is determined by SR correlations between dipoles, in line with Kirkwood’s original arguments.⁴⁷ By construction, SCA accurately describes such SR correlations, from which one can infer that ϵ is indeed the same as for the full system.

The above argument skirts around a subtle issue that, as will be discussed in more detail below, manifests itself as an inconsistency in the response of the SCA system to uniform fields vs. the $\mathbf{k} \rightarrow \mathbf{0}$ limit of its external susceptibility, where \mathbf{k} is a reciprocal space wavevector. One might therefore already anticipate problems where inhomogeneous systems are concerned. Fortunately, the framework provided by LMFT accounts for such inconsistencies on average. Moreover, it will also be shown that the fluctuations deviate from those of the full system in a predictable manner consistent with dielectric continuum theory (DCT).

DIELECTRIC RESPONSE OF BULK LIQUID WATER

An infinite system is not a realizable object, even in a computer simulation that employs PBC. Thus while ϵ can be ‘determined’ within the SCA framework from arguments based on an infinite sample, it still needs to be established how measurable quantities like the polarization response, or fluctuations at zero field, are affected. In this section, such properties will be investigated for bulk liquid water under PBC. This is probably the closest realizable system to the infinite geometry considered above. Nevertheless, it is important to bear in mind that there is now an implicit ‘boundary at infinity’.^{19,20,22,46}

Figures 1 (a) and (b) show how the polarization P responds to either a uniform electric field E or electric displacement field D applied along z , respectively (see e.g. Refs. 48–50). Results are shown both for the case that LR electrostatics are calculated explicitly (‘Ewald’) or neglected entirely (‘SCA’). In fact, using SCA instead of a full LMFT treatment can perhaps be justified here: $\mathcal{V}_R = \mathcal{V}$ on account of the fact that uniform fields only induce charge density at physical boundaries, which, at least explicitly, are absent in the current geometry. ($-\partial_z \mathcal{V} = E$ or D accordingly.) At constant E a degree of non-linear response is observed at larger fields, while the response to constant D is linear to an excellent approximation. In either case, the Ewald and SCA approaches are virtually indistinguishable over the range of field strengths studied. This observation is corroborated

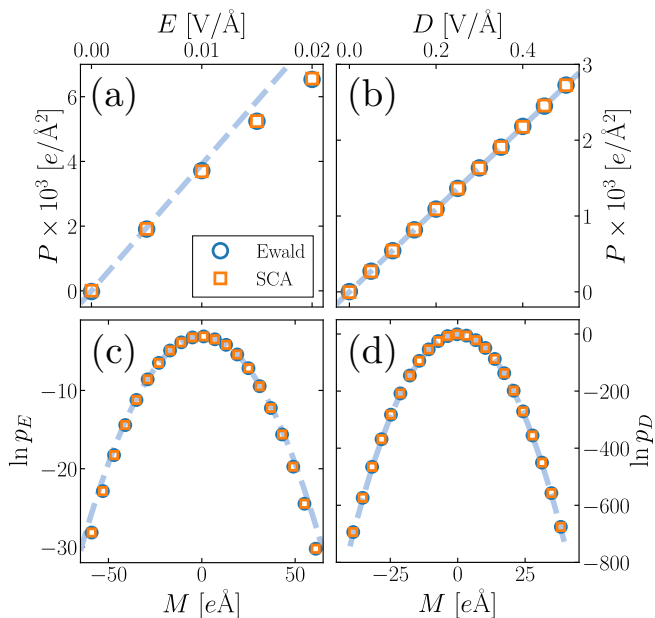


FIG. 1. Dielectric response in homogeneous bulk water. (a) and (b) show respectively the polarization response P to imposed E and D fields (along z). (c) and (d) show respectively the probability distribution of M at $\mathbf{E} = \mathbf{0}$ and $\mathbf{D} = \mathbf{0}$. Agreement between SCA and Ewald is excellent. Dashed lines indicate the expected response [(a) and (b)] or variance [(c) and (d)] from DCT using $\epsilon = 71.7$ (see Fig. 2 and Eq. 6).

by the probability distributions at zero field, p_E and p_D , of the z -component of the total dipole moment of the simulation cell $M = \Omega P$, shown in Figs. 1(c) and (d). (Ω is the volume of the simulation cell.) These have been obtained with histogram reweighting, and in the case of p_D , the wings of the distribution extend far beyond values of P suggested by Fig. 1(b). The agreement between the SCA and Ewald results is remarkable.

The observation that $\langle M^2 \rangle$ obtained from SCA agrees well with Ewald echoes previous studies using Wolf-based electrostatics⁵¹ to compute ϵ .^{52–56} These studies appealed to the seminal works of Neumann and Steinhauser,^{21,24,25} arguing that the fluctuation formula relating $\langle M^2 \rangle$ to ϵ is largely unaffected when using Wolf-based approaches. Instead of following a similar strategy here, the underlying premise of LMFT—to devise a mimic system that accurately captures the SR correlations of the full system—lends itself more naturally to analysis in terms of Caillol’s results,⁴⁶ which prescribe the asymptotic forms of the pair correlation functions of polar fluids under different boundary conditions.

For a cubic simulation cell ($\Omega = L^3$) under PBC, the electrostatic interactions that enter the Hamiltonian are

replaced with the Ewald potential,

$$\psi^{(\lambda)}(\mathbf{r}) = \sum_{\mathbf{n}} \frac{\text{erfc}(\kappa|\mathbf{r} + \mathbf{n}L|)}{|\mathbf{r} + \mathbf{n}L|} + \frac{1}{L^3} \sum_{\mathbf{k} \neq 0} \frac{4\pi}{k^2} e^{i\mathbf{k} \cdot \mathbf{r}} e^{-k^2/4\kappa^2} - \frac{2\pi\lambda}{3} \frac{|\mathbf{r}|^2}{L^3}, \quad (4)$$

where \mathbf{n} is a vector of integers, and $\lambda = 3/(2\epsilon' + 1)$. The dielectric constant ϵ' describes the surrounding medium ‘at infinity’. In SCA, κ^{-1} is chosen sufficiently large such that the sum in reciprocal space can be ignored without affecting the short-range correlations in the system,

$$\psi_{\text{SCA}}^{(\lambda)}(\mathbf{r}) = \sum_{\mathbf{n}} \frac{\text{erfc}(\kappa|\mathbf{r} + \mathbf{n}L|)}{|\mathbf{r} + \mathbf{n}L|} - \frac{2\pi\lambda}{3} \frac{|\mathbf{r}|^2}{L^3}. \quad (5)$$

As Eq. 4 is the Green’s function for the full system, it is clear that the charge distribution has been modified by SCA. This is most easily seen under tin-foil boundary conditions, $\lambda = 0$. In this case $\psi^{(0)}$ describes a periodic set of unit point charges, each embedded in its own homogeneous compensating charge, while $\psi_{\text{SCA}}^{(0)}$ is instead the Green’s function for a set of periodic unit point charges each embedded in its own Gaussian compensating charge (see Supporting Information). Crucially, SCA does not alter the boundary condition at infinity, i.e. the λ -containing terms in Eqs. 4 and 5 are identical. Moreover, the boundary at infinity does not induce structural perturbations, i.e. $n_R = 0$.

The Kirkwood G -factor, $G_K(r) = \langle \boldsymbol{\mu}_1 \cdot \mathbf{M}_v \rangle / \mu^2$, describes orientational correlations between dipoles in the system, where $\boldsymbol{\mu}_1$ is a dipole at the origin, and \mathbf{M}_v is the total dipole moment of a volume v . In order to understand SCA’s performance under PBC, three key results from Ref. 46 are required. The first relates G_K to ϵ and ϵ' ,

$$yG_K(r) = \frac{(2\epsilon + 1)(\epsilon - 1)}{9\epsilon} + \frac{(\epsilon - 1)^2}{9\epsilon} \frac{2(\epsilon' - \epsilon)}{2\epsilon' + \epsilon} \frac{v(r)}{L^3}. \quad (6)$$

The volume v can either be a sphere of radius r , or a cube of dimension r . Setting $v = L^3$ gives the appropriate fluctuation formula relating $\langle |\mathbf{M}|^2 \rangle$ and ϵ for a given ϵ' . The second is the relation between G_K and h_Δ ,

$$G_K(r) = 1 + \frac{\rho}{3} \int_0^r dr' \frac{dv}{dr'} h_\Delta(r'). \quad (7)$$

The third gives the asymptotic behavior of h_Δ which, unlike the infinite system, is now finite,

$$h_\Delta(r) \sim \frac{1}{3y\rho} \frac{(\epsilon - 1)^2}{\epsilon} \frac{2(\epsilon' - \epsilon)}{\epsilon(2\epsilon' + \epsilon)} \frac{1}{L^3}. \quad (8)$$

This finite asymptotic value is clearly a finite size effect, vanishing in the limit $L \rightarrow \infty$.⁵⁷ As it has already been argued that both ϵ and ϵ' are unchanged by SCA, it directly follows that G_K , and thus $\langle |\mathbf{M}|^2 \rangle$, are also unaffected.

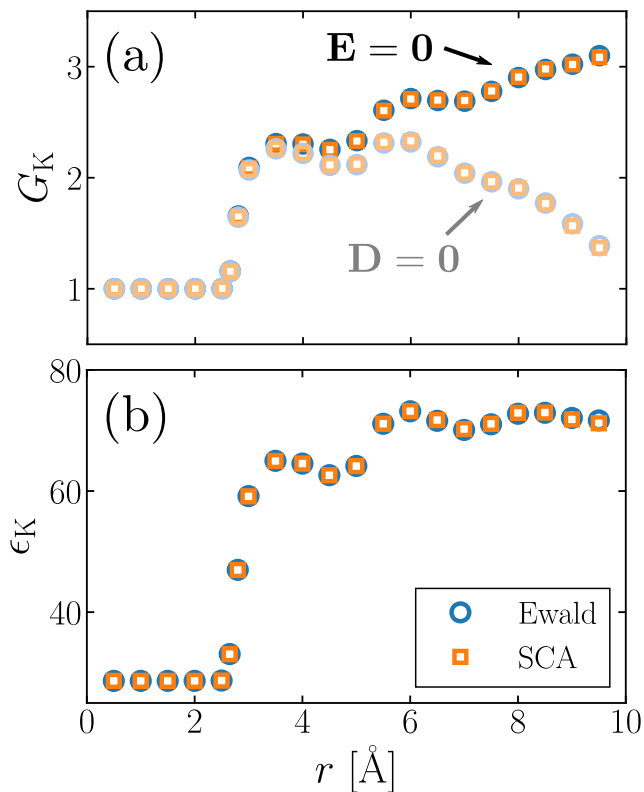


FIG. 2. SR orientational correlations determine ϵ . (a) Kirkwood G -factors obtained at $\mathbf{E} = \mathbf{0}$ ($\epsilon' = \infty$) and $\mathbf{D} = \mathbf{0}$ ($\epsilon' = 0$) have an asymptotic form determined by Eq. 6. (b) Distance dependent dielectric constant ϵ_K obtained from the composite G -factor (see text). Averaging results for $r > \ell_\epsilon = 6$ Å gives $\epsilon = 71.7$ for both Ewald and SCA.

The above arguments suggest that, despite h_Δ 's non-vanishing asymptotic behavior, it can still be considered a SR correlation function amenable to SCA. Further empirical support for such a notion is provided by Fig. 2(a), where G_K is presented for different spherical subvolumes $v = 4\pi r^3/3$. Results are shown for both $\mathbf{E} = \mathbf{0}$ and $\mathbf{D} = \mathbf{0}$, corresponding to $\epsilon' = \infty$ and $\epsilon' = 0$, respectively.^{48,49} G_K obtained from SCA is virtually indistinguishable compared to the Ewald result. Following Ref. 49, the distance dependent dielectric constant $\epsilon_K(r)$ can be found from the asymptotic value of the composite Kirkwood G -factor, $G_{Kc} = (2G_{K,\mathbf{E}=\mathbf{0}} + G_{K,\mathbf{D}=\mathbf{0}})/3$. This result is presented in Fig. 2(b). Averaging ϵ_K for $r > 6$ Å = ℓ_ϵ gives the macroscopic static dielectric constant: $\epsilon = 71.7$ for both the SCA and Ewald systems. This is in good agreement with existing literature values for SPC/E water.^{48–50,58–60} The dashed lines in Fig. 1 indicate the expected response [(a) and (b)] or variance [(c) and (d)] from DCT using $\epsilon = 71.7$.

The results presented so far suggest a near flawless performance of SCA in describing the dielectric properties of polar liquids like water. While this is entirely consistent with the principle that ϵ is determined by

SR orientational correlations, it is still nonetheless remarkable given the history associated with proper account of LR electrostatics.^{19–28} In fact, it is not immediately obvious that Eqs. 3 and 6 should hold within the SCA framework: The factor $(2\epsilon + 1)(\epsilon - 1)/9\epsilon$ originates from the trace of the anisotropic external susceptibility $\chi^{(0)}(\mathbf{k}) \propto \langle \tilde{\mathbf{m}}(\mathbf{k})\tilde{\mathbf{m}}^*(\mathbf{k}) \rangle$ in the $\mathbf{k} \rightarrow 0$ limit,⁴⁵ while for a system comprising exclusively SR interactions, one would expect $\chi^{(0)}$ to be isotropic at long wavelengths. ($\tilde{\mathbf{m}}$ is the Fourier transform of the molecular dipole density, using the water oxygen atom as the molecular center.) Such behavior is indeed hinted at by Fig. 3, where $\langle \tilde{m}_\alpha(k)\tilde{m}_\alpha^*(k) \rangle$ is shown, with $\alpha = x, y, z$ and $\mathbf{k} = k\hat{\mathbf{z}}$. While for the best part good agreement between the SCA and Ewald approaches is seen, discrepancies are observed at long wavelengths in the longitudinal ($\alpha = z$) fluctuations, with the SCA results sharply increasing as $k \rightarrow 0$. It is interesting that these deviations appear at length scales far larger than the range separation prescribed by SCA (see inset).

In a full treatment of electrostatics, setting $\mathbf{E} = \mathbf{0}$ ensures $\chi_{xx}^{(0)}$ and $\chi_{yy}^{(0)}$ are continuous at $k = 0$, e.g. $\chi_{xx}^{(0)}(k \rightarrow 0) = \chi_{xx}^{(0)}(0)$. On the other hand, $\chi_{zz}^{(0)}$ is discontinuous i.e. $\chi_{zz}^{(0)}(k \rightarrow 0) \neq \chi_{zz}^{(0)}(0)$.²³ The situation is reversed for $\mathbf{D} = \mathbf{0}$. In contrast, Fig. 3 suggests that with SCA, $\chi_{\alpha\alpha}^{(0)}(k \rightarrow 0) = \chi_{\alpha\alpha}^{(0)}(0)$ at $\mathbf{E} = \mathbf{0}$ and $\chi_{\alpha\alpha}^{(0)}(k \rightarrow 0) \neq \chi_{\alpha\alpha}^{(0)}(0)$ at $\mathbf{D} = \mathbf{0}$, irrespective of whether $\alpha = x, y$ or z . The fact that $\mathbf{k} = \mathbf{0}$ response to both \mathbf{E} and \mathbf{D} in SCA well describes that of the full system therefore suggests an inconsistency within the SCA framework. We will see the consequences of this when considering an inhomogeneous system below. There it will also be shown that the $k \rightarrow 0$ longitudinal and transverse external susceptibilities are indeed equal in SCA i.e. the former is too large by a factor ϵ . (See also Supporting Information.) Fortunately, LMFT readily provides a route to account for this inconsistency.

DIELECTRIC RESPONSE WITH EXTENDED INTERFACES

Placing systems under PBC is a useful construction for investigating bulk properties of materials such as ϵ , especially when computational resources are limited. Real systems, however, have boundaries that will induce structural inhomogeneities. These structural inhomogeneities may also be accompanied by regions of non-vanishing charge density of the polar liquid. This could arise from the boundary itself preferentially orienting the molecules of the liquid (e.g. due to functional groups at a solid surface), or from an asymmetric charge distribution in the liquid's constituent molecules (e.g. water). In any event, it is simply not enough to evaluate the performance of SR interaction potentials on their ability to reproduce properties of homogeneous systems. Rather, it is imperative to assess and understand their behavior in the presence of extended interfaces.

In this section, the dielectric properties of water confined between structureless, repulsive walls will be investigated. This is a prototypical model for understanding nanoconfined water in hydrophobic environments. In such a geometry, the interface is approximately planar, and Eq. 2 can be recast as

$$\mathcal{V}_R(z) = \mathcal{V}(z) + \frac{1}{L} \sum_{k \neq 0} \frac{4\pi}{k^2} \tilde{n}_R(k) \exp(ikz) \exp(-k^2/4\kappa^2), \quad (9)$$

where \tilde{n}_R denotes a Fourier component of n_R , and L is now the total length of the simulation cell in the direction perpendicular to the interface (taken to be z). The system is still understood to be replicated in all three dimensions. A schematic is shown in Fig. 4 (a).

Even in the absence of an external field, liquid water has a non-vanishing charge density close to the interface. Consequently, \mathcal{V}_R is finite, along with a corresponding restructuring field $\mathcal{E}_R = -\partial_z \mathcal{V}_R$. Neglecting \mathcal{E}_R has severe consequences for the orientational statistics of water in a confined geometry. This was already discussed by Rodgers and Weeks³⁰ and their results are recapitulated in a slightly different form in Fig. 4 (b), where the average molecular dipole density along z is shown. While the average polarization obtained with LMFT agrees well with the Ewald system, the SCA system on its own ($\mathcal{E}_R = 0$) yields a qualitatively incorrect picture. Crucial to what follows is that LMFT also gives the correct average polarization in the presence of a uniform field, which is also shown in Fig. 4 (b) for $D = -\partial_z \mathcal{V} = 0.15 \text{ V/\AA}$.

It is clear that LMFT provides a means to correct for the effects of neglecting LR electrostatics on the average dielectric response in inhomogeneous systems. Re-

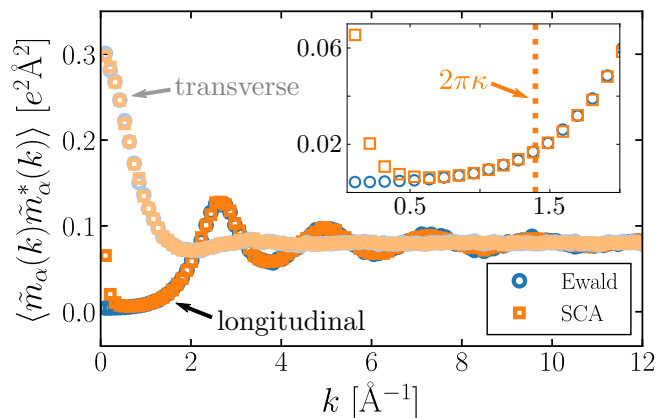


FIG. 3. Dipole density correlations in reciprocal space $\langle \tilde{m}_\alpha(k) \tilde{m}_\alpha^*(k) \rangle$ determined for both Ewald and SCA electrostatics ($\alpha = x, y, z$, and $\mathbf{k} = k\hat{z}$). On the whole, good agreement between SCA and Ewald is seen. Inset: At low k , SCA's longitudinal correlations ($\alpha = z$) deviate from Ewald, tending toward the transverse correlations ($\alpha = x, y$). These deviations occur on a length scale greater than the range separation prescribed by SCA, as indicated by the vertical dotted line at $k = 2\pi\kappa$.

sults from previous studies^{61–65} suggest the fluctuations will also be affected, and establishing how they are affected is likely to provide useful physical insight. To set about tackling this issue, let us consider a continuum model in which a uniform dielectric slab with thickness w is centered at $z = 0$ such that its boundaries occur at $z_\pm = \pm w/2$. A vacuum region exists either side of the slab. If the slab has a uniform polarization P , this leads to a charge density at the boundaries, $n(z) = P[\delta(z - w/2) - \delta(z + w/2)]$. Recalling that $n_R = n$ at self-consistency, taking the Fourier transform of n , substituting into Eq. 9 and differentiating to find \mathcal{E}_R gives

$$\mathcal{E}_R(z) = \mathcal{E}(z) - \frac{8\pi P}{L} \sum_{k \neq 0} \frac{\cos(kz) \sin(kw/2)}{k} \exp(-k^2/4\kappa^2). \quad (10)$$

In the limit $L \rightarrow \infty$, this can be solved analytically,

$$\lim_{L \rightarrow \infty} \mathcal{E}_R(z) = \mathcal{E}(z) - 2\pi P \left\{ \operatorname{erf}[(w/2 - z)\kappa] + \operatorname{erf}[(w/2 + z)\kappa] \right\}. \quad (11)$$

In this case it is instructive to consider the limiting values of κ ,

$$\mathcal{E}_R(z) = \begin{cases} \mathcal{E}(z) & (\text{as } \kappa \rightarrow 0), \\ \mathcal{E}(z) - 4\pi P & (\text{as } \kappa \rightarrow \infty). \end{cases} \quad (12a) \quad (12b)$$

The result for $\kappa \rightarrow 0$ simply states that all electrostatic interactions have been accounted for explicitly in the SCA system. In the case $\kappa \rightarrow \infty$, the result can be interpreted as follows: Due to the neglect of LR electrostatics, the SCA system omits the depolarizing field established by the induced surface charge density at the boundaries, which is then accounted for by the second term ($-4\pi P$) in Eq. 12b. For finite κ , it is found empirically that $\mathcal{E}_R = \mathcal{E} - 4\pi P$ is an excellent approximation in the slab's interior, provided $w \gg \kappa^{-1}$. In the general case of finite L , Eq. 10 can be solved numerically in a straightforward manner. This is shown in Fig. 4 (c) for $L = 75, 150$, and 300 \AA , along with the analytic result (Eq. 11) for $L \rightarrow \infty$, using $\epsilon = 71.7$ obtained above. Also shown is \mathcal{E}_R for $L = 75 \text{ \AA}$ obtained from simulation, with the spontaneous contribution subtracted (see Supporting Information). The simple dielectric continuum model presented above captures this result from molecular simulation with remarkable accuracy.

When subjected to an external field along z , the slab responds according to its longitudinal external susceptibility,

$$4\pi P = 4\pi \chi_{zz}^{(0)} \mathcal{E} = \left(\frac{\epsilon - 1}{\epsilon} \right) \mathcal{E}. \quad (13)$$

By construction, LMFT gives the same P as the full system. The field it responds to, however, is \mathcal{E}_R rather than

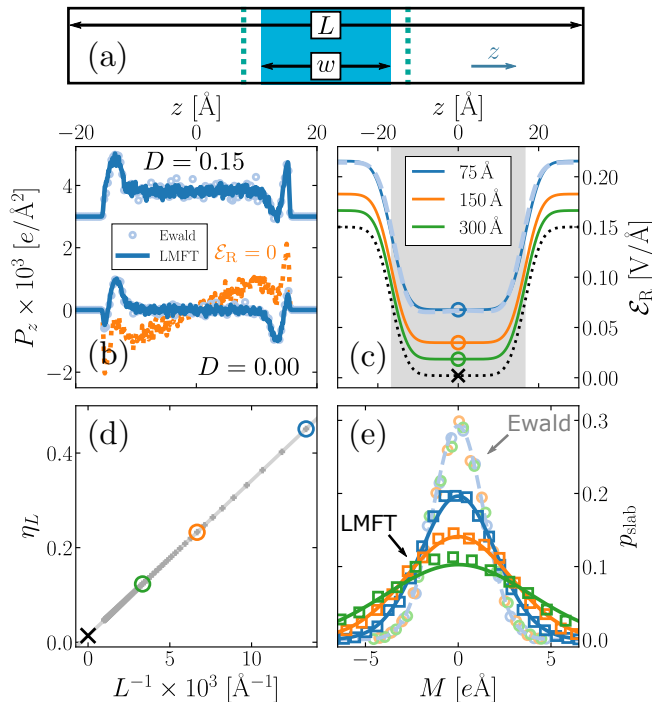


FIG. 4. Dielectric response of water confined between hydrophobic walls, shown schematically in (a). A water slab of thickness w , centered at $z = 0$, forms two interfaces with vacuum in the xy -plane at $z = \pm w/2$. L denotes the total length of the simulation cell along z . The dotted lines depict the confining walls. (b) Average polarization profiles P_z at both $D = 0$ and $D = 0.15 \text{ V/\AA}$ (shifted vertically by $3 \times 10^3 \text{ e/\AA}^2$ for clarity) are well described by LMFT. Neglecting \mathcal{E}_R at $D = 0$ results in poor agreement, as indicated by the orange dotted line. (c) \mathcal{E}_R predicted by DCT with $\mathcal{E} = 0.15 \text{ V/\AA}$, $\epsilon = 71.7$ and $w = 33.2 \text{ \AA}$. Solid lines have been obtained by numerically evaluating Eq. 10 for finite L (see legend). The dashed line is a simulation result for $L = 75 \text{ \AA}$, with the spontaneous contribution subtracted. The dotted line shows the $L \rightarrow \infty$ result (Eq. 11). The shaded region indicates $-w/2 \leq z \leq w/2$. (d) η_L vs L^{-1} obtained by evaluating Eq. 10 at $z = 0$ [see open circles in (c)]. The solid line is a linear fit. The black cross indicates $\eta_\infty = 1/\epsilon$. (e) Probability distributions of the slab's dipole moment. With Ewald, this is relatively insensitive to L . With LMFT, DCT predicts the variance increases as η_L^{-1} , as indicated by the solid lines.

\mathcal{E} ,

$$4\pi P = 4\pi\chi_{R,zz}^{(0)}\mathcal{E}_R \approx 4\pi\chi_{R,zz}^{(0)}\eta_L\mathcal{E}, \quad (14)$$

where $\eta_L \leq 1$ is an L -dependent scalar relating \mathcal{E}_R to \mathcal{E} , and the relationship is approximate as variations close to the boundaries are ignored. By evaluating Eq. 10 at $z = 0$, η_L is found to scale linearly with $1/L$, as seen in Figs. 4(c) and (d). In the limit $L \rightarrow \infty$, substituting Eq. 12b gives $4\pi P = 4\pi\chi_{R,zz}^{(0)}[\mathcal{E} - 4\pi P]$. Substituting Eq. 13 and rearranging yields,

$$\lim_{L \rightarrow \infty} 4\pi\chi_{R,zz}^{(0)} = \epsilon - 1. \quad (15)$$

Comparing with Eqs. 13 and 14, it is clear that $\eta_\infty = 1/\epsilon$. Thus it is indeed the case that the longitudinal external susceptibility is too large by factor ϵ as $k \rightarrow 0$. (See also Supporting Information.)

This simple dielectric continuum model directly elicits information on the fluctuations in the LMFT formalism. Specifically, it immediately follows that $\langle M^2 \rangle$ in LMFT is a factor $1/\eta_L$ larger than it is with Ewald. This is confirmed in Fig. 4(e), where the probability distributions of M for the slab p_{slab} obtained from simulations with different L are plotted along with Gaussian distributions with variances predicted by this dielectric continuum model. It is stressed that these are not fits to the simulation data: $\epsilon = 71.7$ has been determined from the simulations of bulk water, and $w = 33.2 \text{ \AA}$ has been determined from the variance of p_{slab} obtained using Ewald sums (see Supporting Information). The fact that this simple DCT model describes the behavior of the LMFT system so well is further support for the notion that ϵ is unchanged from that of the system with full electrostatics.

DISCUSSION

LMFT provides an elegant statistical mechanical framework that is readily compatible with standard molecular simulation approaches, and can be applied in cases when it is not always clear, at least *a priori*, that conventional mean field treatments will work. Improving our theoretical descriptions of solvation is one area where LMFT has enjoyed much recent success.^{38,39,66} This includes both hydrophobic and ionic solvation across a range of length scales. As the solvent's dielectric constant plays a central role in our understanding of solvation, particularly in the case of charged solutes, the results presented above lend further weight to LMFT as a suitable approach for investigating solvation, and should facilitate its development going forward.

Of particular relevance to this work is the recent study of Gao *et al.*, in which LMFT was used to probe ion correlations in water.³⁹ It was found that treating all electrostatic interactions with the SR v_0 led to potential of mean forces (PMFs) that disagreed with a full electrostatic treatment. This was attributed to the inability of this ' v_0 -only' approach to capture effects of dielectric screening on the PMFs. Building on results from Remsing *et al.*,³⁸ this discrepancy was corrected by introducing a renormalized direct ion-ion interaction, which was shown to have an asymptotic limit ($\sim 1/\epsilon r$) consistent with DCT. A pleasing aspect of the results presented above is that they show this renormalized interaction is consistent with the static dielectric constant of the underlying SR solvent. The same can also be said for corrections to thermodynamic properties of uniform systems, e.g. the internal energy and pressure, that depend on ϵ .⁴⁴

The fact that certain dielectric properties of polar liquids can be captured with SR interaction potentials could

be highly advantageous to those seeking to describe liquids without explicit reference to LR electrostatic interactions. It is abundantly clear, however, that the effects of LR electrostatics cannot simply be neglected entirely. This was already obvious from early LMFT studies on liquid water, even in the absence of external fields.^{30,67} It is also clear that the polarization fluctuations of inhomogeneous systems will also be affected, which could have been anticipated from previous studies. In particular, symmetry-preserving mean-field theory (an extension of LMFT)^{61–64} likely provides a means to recover the fluctuations by capturing both equilibrium and dynamical effects of interfaces with high symmetry (see also Ref. 65). In this article, no such attempt to correct the fluctuations in LMFT has been made. Instead, it has been demonstrated that dielectric properties of a system with SR electrostatic interactions are described well by DCT where ϵ is unchanged from that of a system with full electrostatics.

Earlier in this article, it was taken as given that ϵ is an intensive quantity that does not depend upon sample shape. While this is supported by rigorous theoretical calculations (see e.g. Ref. 68), the fact that dielectric properties can be understood within the LMFT framework can be viewed as a demonstration of this result, and is perhaps more open to intuitive physical interpretation. This may prove useful as we continue to develop our understanding of dielectrics under confinement.^{1,4,9,10}

METHODS

All simulations used the SPC/E water model,⁶⁹ whose geometry was constrained using the RATTLE algorithm.⁷⁰ Dynamics were propagated using the velocity Verlet algorithm with a time step of 2 fs. The temperature was maintained at 298 K with a Nosé-Hoover chain,^{71,72} with a damping constant 0.2 ps. Where applicable, the particle-particle particle-mesh Ewald method was used to account for long-ranged interactions,⁷³ with parameters chosen such that the root mean square error in the forces were a factor 10^5 smaller than the force between two unit charges separated by a distance of 1.0 Å.⁷⁴ A cutoff of 10 Å was used for non-electrostatic interactions: For simulations using LMFT/SCA, this cutoff was used for all interactions. The LAMMPS simulation package was used throughout.⁷⁵ For simulations with an imposed electric displacement field, the implementation given in Ref. 50 was used. Simulations using LMFT/SCA required further modification of the LAMMPS source code, which has been made freely available.

For results presented in Fig. 1, the system comprised 256 molecules in a cubic simulation cell of dimension $L = 19.7304$ Å. For Figs. 1 (b) and (d), an electric displacement field was imposed in all three dimensions i.e. $\mathbf{D} = D_x \hat{\mathbf{x}} + D_y \hat{\mathbf{y}} + D_z \hat{\mathbf{z}}$ with $D_x = D_y = 0$. See Ref. 48 for further discussion of this point. Simulations at constant \mathbf{E} were run for 150 ns post equilibration, while those at constant \mathbf{D} were run between 2.5 ns and 5.0 ns. The probability distributions p_E and p_D were obtained using the multistate Bennett acceptance ratio method,⁷⁶ with simulations performed at $E = 0, \pm 0.005, \dots, \pm 0.020$ V/Å, and $D = 0, \pm 0.05, \dots, \pm 1.45$ V/Å, respectively. The Kirkwood G -factors (Fig. 2) were obtained from the same set of simulations, although those at $\mathbf{E} = \mathbf{0}$ were performed for a further 150 ns with configurations stored more frequently (every 30 ps). Results presented in Fig. 3 were obtained from 45–50 ns simulations of 6912 molecules with $L = 59.1912$ Å and $\mathbf{D} = \mathbf{0}$.

For simulations of water between hydrophobic walls (Fig. 4), 400 water molecules were confined between Lennard-Jones 9-3 walls,

$$u_{\text{wall}}(z) = \epsilon_w \left[\frac{2}{15} \left(\frac{\sigma_w}{\Delta_{\text{lo}z}} \right)^9 - \left(\frac{\sigma_w}{\Delta_{\text{lo}z}} \right)^3 \right] + \epsilon_w \left[\frac{2}{15} \left(\frac{\sigma_w}{\Delta_{\text{hi}z}} \right)^9 - \left(\frac{\sigma_w}{\Delta_{\text{hi}z}} \right)^3 \right], \quad (16)$$

where $\Delta_{\text{lo}z} = |z - z_{\text{lo}}|$ and $\Delta_{\text{hi}z} = |z - z_{\text{hi}}|$ with $z_{\text{lo}} \leq z \leq z_{\text{hi}}$ located within the primary simulation cell. All simulations used $z_{\text{hi}} = -z_{\text{lo}} = 17.25$ Å, $\epsilon_w = 0.6$ kcal/mol and $\sigma_w = 2.5$ Å. The potential was truncated and shifted for $\Delta_{\text{lo}(\text{hi})z} \geq 2.1459$ Å. Simulations were between 25 ns and ~ 90 ns. Hybrid boundary conditions were used⁴⁸ i.e. $\mathbf{D} = D\hat{\mathbf{z}}$ and $E_x = E_y = 0$. For $D = 0$, this is formally equivalent to the Yeh-Berkowitz correction for the slab geometry.⁷⁷

ACKNOWLEDGMENTS

Michiel Sprik and Rob Jack are thanked for insightful discussions. Simón Ramírez-Hinestrosa is thanked for technical discussions regarding the LAMMPS implementation. Computational support from the UK Materials and Molecular Modelling Hub, which is partially funded by EPSRC (EP/P020194), for which access was obtained via the UKCP consortium and funded by EPSRC grant ref EP/P022561/1, is gratefully acknowledged. I am supported by a Royal Commission for the Exhibition of 1851 Research Fellowship.

DATA AVAILABILITY

Source code beyond the standard LAMMPS distribution used to perform simulations described here can be accessed at <https://github.com/uccasco/LMFT>. Input files for the simulations are openly available at the University of Cambridge Data Repository, <https://doi.org/10.17863/CAM.52565>.

The published version of this article can be found at <https://doi.org/10.1073/pnas.2005847117>.

- ¹L. Fumagalli, A. Esfandiari, R. Fabregas, S. Hu, P. Ares, A. Jannardanan, Q. Yang, B. Radha, T. Taniguchi, K. Watanabe, G. Gomila, K. S. Novoselov, and A. K. Geim, *Science* **360**, 1339 (2018).
- ²Y. Chen, H. I. Okur, N. Gomopoulos, C. Macias-Romero, P. S. Cremer, P. B. Petersen, G. Tocci, D. M. Wilkins, C. Liang, M. Ceriotti, and S. Roke, *Sci. Adv.* **2**, e1501891 (2016).
- ³D. P. Shelton, *J. Chem. Phys.* **147**, 214505 (2017).
- ⁴C. Zhang, *J. Chem. Phys.* **148**, 156101 (2018).
- ⁵S. Seyedi, D. R. Martin, and D. V. Matyushov, *J. Phys: Condens. Matter* **31**, 325101 (2019).
- ⁶H. Berthoumieux and F. Paillusson, *J. Chem. Phys.* **150**, 094507 (2019).
- ⁷E. Pluharová, D. Laage, and P. Jungwirth, *J. Phys. Chem. Lett.* **8**, 2031 (2017).
- ⁸L. Belloni, D. Borgis, and M. Levesque, *J. Phys. Chem. Lett.* **9**, 1985 (2018).
- ⁹A. Schlaich, E. W. Knapp, and R. R. Netz, *Phys. Rev. Lett.* **117**, 048001 (2016).

- ¹⁰P. Loche, C. Ayaz, A. Wolde-Kidan, A. Schlaich, and R. R. Netz, *J. Phys. Chem. B* **124**, 4365 (2020).
- ¹¹R. C. Remsing and J. D. Weeks, *J. Phys. Chem. B* **120**, 6238 (2016).
- ¹²R. Zhao, R. C. Remsing, and J. D. Weeks, *J. Stat. Phys.* (2020), 10.1007/s10955-020-02509-z.
- ¹³S. J. Cox and P. L. Geissler, *J. Chem. Phys.* **148**, 222823 (2018).
- ¹⁴H. Fröhlich, *Theory of Dielectrics: Dielectric Constant and Dielectric Loss*, 2nd ed. (Oxford University Press, Oxford, United Kingdom, 1958).
- ¹⁵S. Leikin, V. A. Parsegian, D. C. Rau, and R. P. Rand, *Annu. Rev. Phys. Chem.* **44**, 369 (1993).
- ¹⁶D. Bashford and D. A. Case, *Annu. Rev. Phys. Chem.* **51**, 129 (2000).
- ¹⁷B. Roux, T. Allen, S. Bernèche, and W. Im, *Q. Rev. Biophys.* **37**, 15 (2004).
- ¹⁸B. Honig and A. Nicholls, *Science* **268**, 1144 (1995).
- ¹⁹S. W. de Leeuw, J. W. Perram, and E. R. Smith, *Proc. R. Soc. London A* **373**, 27 (1980).
- ²⁰S. W. de Leeuw, J. W. Perram, and E. R. Smith, *Proc. R. Soc. London A* **373**, 57 (1980).
- ²¹M. Neumann, *Mol. Phys.* **50**, 841 (1983).
- ²²S. De Leeuw, J. W. Perram, and E. R. Smith, *Annu. Rev. Phys. Chem.* **37**, 245 (1986).
- ²³M. Neumann, *Mol. Phys.* **57**, 97 (1986).
- ²⁴M. Neumann and O. Steinhauser, *Chem. Phys. Lett.* **95**, 417 (1983).
- ²⁵M. Neumann and O. Steinhauser, *Chem. Phys. Lett.* **102**, 508 (1983).
- ²⁶M. Neumann and O. Steinhauser, *Chem. Phys. Lett.* **106**, 563 (1984).
- ²⁷E. R. Smith, *Proc. R. Soc. London A* **375**, 475 (1981).
- ²⁸V. Ballenegger, *J. Chem. Phys.* **140**, 161102 (2014).
- ²⁹C. J. Fennell and J. D. Gezelter, *J. Chem. Phys.* **124**, 234104 (2006).
- ³⁰J. M. Rodgers and J. D. Weeks, *Proc. Natl. Acad. Sci. USA* **105**, 19136 (2008).
- ³¹J. M. Rodgers and J. D. Weeks, *J. Phys: Condens. Matter* **20**, 494206 (2008).
- ³²L. Zhang, J. Han, H. Wang, R. Car, and E. Weinan, *Phys. Rev. Lett.* **120**, 143001 (2018).
- ³³B. Cheng, E. A. Engel, J. Behler, C. Dellago, and M. Ceriotti, *Proc. Natl. Acad. Sci. USA* **116**, 1110 (2019).
- ³⁴Y. Zuo, C. Chen, X. Li, Z. Deng, Y. Chen, J. Behler, G. Csányi, A. V. Shapeev, A. P. Thompson, M. A. Wood, *et al.*, *J. Phys. Chem. A* **124**, 731 (2020).
- ³⁵A. Grisafi and M. Ceriotti, *J. Chem. Phys.* **151**, 204105 (2019).
- ³⁶A. Grisafi, D. M. Wilkins, G. Csányi, and M. Ceriotti, *Phys. Rev. Lett.* **120**, 036002 (2018).
- ³⁷A. J. Archer and R. Evans, *J. Chem. Phys.* **138**, 014502 (2013).
- ³⁸R. C. Remsing, S. Liu, and J. D. Weeks, *Proc. Natl. Acad. Sci. USA* **113**, 2819 (2016).
- ³⁹A. Gao, R. C. Remsing, and J. D. Weeks, *Proc. Natl. Acad. Sci. USA* **117** (2020).
- ⁴⁰J. D. Weeks, *Annu. Rev. Phys. Chem.* **53**, 533 (2002).
- ⁴¹Z. Hu and J. D. Weeks, *Phys. Rev. Lett.* **105**, 140602 (2010).
- ⁴²J. M. Rodgers, Z. Hu, and J. D. Weeks, *Mol. Phys.* **109**, 1195 (2011).
- ⁴³K. Vollmayr-Lee, K. Katsov, and J. D. Weeks, *J. Chem. Phys.* **114**, 416 (2001).
- ⁴⁴J. M. Rodgers and J. D. Weeks, *J. Chem. Phys.* **131**, 244108 (2009).
- ⁴⁵P. Madden and D. Kivelson, "A consistent molecular treatment of dielectric phenomena," in *Adv. Chem. Phys.* (John Wiley & Sons, Inc., 1984) pp. 467–566.
- ⁴⁶J. M. Caillol, *J. Chem. Phys.* **96**, 7039 (1992).
- ⁴⁷J. G. Kirkwood, *J. Chem. Phys.* **7**, 911 (1939).
- ⁴⁸C. Zhang and M. Sprik, *Phys. Rev. B* **93**, 144201 (2016).
- ⁴⁹C. Zhang, J. Hutter, and M. Sprik, *J. Phys. Chem. Lett.* **7**, 2696 (2016).
- ⁵⁰S. J. Cox and M. Sprik, *J. Chem. Phys.* **151**, 064506 (2019).
- ⁵¹D. Wolf, P. Keblinski, S. Phillpot, and J. Eggebrecht, *J. Chem. Phys.* **110**, 8254 (1999).
- ⁵²J. Armstrong and F. Bresme, *J. Chem. Phys.* **139**, 014504 (2013).
- ⁵³D. Zahn, B. Schilling, and S. M. Kast, *J. Phys. Chem. B* **106**, 10725 (2002).
- ⁵⁴Y. Yonezawa, *J. Chem. Phys.* **136**, 06B616 (2012).
- ⁵⁵G. S. Fanourgakis, *J. Phys. Chem. B* **119**, 1974 (2015).
- ⁵⁶Y. Yonezawa, *Chem. Phys. Lett.* **556**, 308 (2013).
- ⁵⁷The asymptotic behavior of h_{Δ} can also be made to vanish by setting $\epsilon' = \epsilon$, which effectively samples the infinite geometry.
- ⁵⁸D. van der Spoel, P. J. van Maaren, and H. J. Berendsen, *J. Chem. Phys.* **108**, 10220 (1998).
- ⁵⁹J. Aragones, L. MacDowell, and C. Vega, *J. Phys. Chem. A* **115**, 5745 (2010).
- ⁶⁰D. Braun, S. Boresch, and O. Steinhauser, *J. Chem. Phys.* **140**, 064107 (2014).
- ⁶¹Z. Hu, *Chem. Commun.* **50**, 14397 (2014).
- ⁶²C. Pan, S. Yi, and Z. Hu, *Phys. Chem. Chem. Phys.* **19**, 4861 (2017).
- ⁶³S. Yi, C. Pan, L. Hu, and Z. Hu, *Phys. Chem. Chem. Phys.* **19**, 18514 (2017).
- ⁶⁴C. Pan, S. Yi, and Z. Hu, *Phys. Chem. Chem. Phys.* **21**, 14858 (2019).
- ⁶⁵E. B. Baker, J. M. Rodgers, and J. D. Weeks, *J. Phys. Chem. B* **124**, 5676 (2020).
- ⁶⁶A. Gao, L. Tan, M. I. Chaudhari, D. Asthagiri, L. R. Pratt, S. B. Rempe, and J. D. Weeks, *J. Phys. Chem. B* **122**, 6272 (2018).
- ⁶⁷R. C. Remsing, J. M. Rodgers, and J. D. Weeks, *J. Stat. Phys.* **145**, 313 (2011).
- ⁶⁸D. Chandler, *J. Chem. Phys.* **67**, 1113 (1977).
- ⁶⁹H. J. C. Berendsen, J. R. Grigera, and T. P. Straatsma, *J. Phys. Chem.* **91**, 6269 (1987).
- ⁷⁰H. C. Andersen, *J. Comput. Phys.* **52**, 24 (1983).
- ⁷¹W. Shinoda, M. Shiga, and M. Mikami, *Phys. Rev. B* **69**, 134103 (2004).
- ⁷²M. E. Tuckerman, J. Alejandre, R. López-Rendón, A. L. Jochim, and G. J. Martyna, *J. Phys. A* **39**, 5629 (2006).
- ⁷³R. W. Hockney and J. W. Eastwood, *Computer simulation using particles* (CRC Press, 1988).
- ⁷⁴J. Kolafa and J. W. Perram, *Mol. Sim.* **9**, 351 (1992).
- ⁷⁵S. Plimpton, *J. Comput. Phys.* **117**, 1 (1995).
- ⁷⁶M. R. Shirts and J. D. Chodera, *J. Chem. Phys.* **129**, 124105 (2008).
- ⁷⁷I.-C. Yeh and M. L. Berkowitz, *J. Chem. Phys.* **111**, 3155 (1999).
- ⁷⁸J.-M. Caillol, *J. Chem. Phys.* **101**, 6080 (1994).

Supporting Information

COMPARING THE DCT MODEL WITH MOLECULAR SIMULATION

Even in the absence of an imposed electric or electric displacement field, water exhibits a non-vanishing charge density close to the interface. Consequently, the restructuring potential Eq. 9 is also non-vanishing. The corresponding restructuring field for the confined system (see Fig. 4) at $D = 0 \text{ V}/\text{\AA}$ is shown by the dotted line in Fig. S1. Also shown by the solid line in Fig. S1 is the full restructuring field at $D = 0.15 \text{ V}/\text{\AA}$. The DCT model presented in the main article aims to describe the response of the confined system to uniform fields, and does not account for effects of the spontaneous charge density at $D = 0 \text{ V}/\text{\AA}$ on \mathcal{E}_R . Thus, when comparing results from molecular simulation to the DCT model, the restructuring field at $D = 0 \text{ V}/\text{\AA}$ needs to be subtracted from the full restructuring field for $D \neq 0$. This results in the dashed line presented in Fig. S1 and Fig. 4(c).

PREDICTING THE VARIANCE OF M FOR CONFINED WATER WITH LMFT

The solid lines shown in Fig. 4(e) are not fits to the simulation data. Rather, they show predictions of the simple DCT model. The value $\epsilon = 71.7$ was obtained from the simulations of bulk water (see Fig. 2). In order to find w , the average variance $\overline{\langle M^2 \rangle}_{\text{ew}}$ from the three Ewald simulations was calculated. Simple electrostatic arguments then give

$$w = \frac{4\pi\beta}{A} \left(\frac{\epsilon}{\epsilon - 1} \right) \overline{\langle M^2 \rangle}_{\text{ew}}, \quad (\text{S1})$$

where A is the cross-sectional area of the slab. For the system under consideration in Fig. 4, this gives $w = 33.2 \text{ \AA}$, which was used in Eqs. 10 and 11 to produce Figs. 4(c) and (d). The Gaussian distributions shown by the solid lines in Fig. 4(e) have zero mean, and variance $\overline{\langle M^2 \rangle}_{\text{ew}}/\eta_L$.

DISCUSSION OF THE GREEN'S FUNCTIONS

Equation 4 gives the Green's function of Poisson's equation in periodic space. This is well established,^{22,46} but it is useful to see this in the present notation before going on to discuss SCA. To this end, note that $\psi^{(\lambda)}$ is independent of κ . For formal manipulations, it is convenient to consider the limit $\kappa \rightarrow \infty$,

$$\psi^{(\lambda)}(\mathbf{r}) = \frac{1}{L^3} \sum_{\mathbf{k} \neq 0} \frac{4\pi}{k^2} e^{i\mathbf{k} \cdot \mathbf{r}} - \frac{2\pi\lambda}{3} \frac{|\mathbf{r}|^2}{L^3}. \quad (\text{S2})$$

Calculating the Laplacian gives

$$\nabla^2 \psi^{(\lambda)}(\mathbf{r}) = -\frac{4\pi}{L^3} \sum_{\mathbf{k} \neq 0} e^{i\mathbf{k} \cdot \mathbf{r}} - \frac{4\pi\lambda}{L^3}, \quad (\text{S3})$$

$$= -\frac{4\pi}{L^3} \sum_{\mathbf{k}} e^{i\mathbf{k} \cdot \mathbf{r}} - \frac{4\pi\lambda}{L^3} + \lim_{\mathbf{k} \rightarrow 0} \frac{4\pi}{L^3} e^{i\mathbf{k} \cdot \mathbf{r}}, \quad (\text{S4})$$

$$= -4\pi \left[\frac{1}{L^3} \sum_{\mathbf{k}} e^{i\mathbf{k} \cdot \mathbf{r}} + \frac{\lambda - 1}{L^3} \right]. \quad (\text{S5})$$

From the completeness relation, $(1/L^3) \sum_{\mathbf{k}} \exp(i\mathbf{k} \cdot \mathbf{r})$ is a set of periodically replicated δ -functions. It is then clear that $\psi^{(\lambda)}$ is the electrostatic potential of a periodically replicated unit point charge embedded in a uniform background charge $(\lambda - 1)/L^3$. Note that the uniform background charge has two contributions: one from the λ -containing term in Eq. 4, and another from the regularization of the Ewald sum i.e. from excluding the $\mathbf{k} = \mathbf{0}$ term in reciprocal space. Indeed, for the familiar tin-foil boundary conditions ($\lambda = 0$),

$$\nabla^2 \psi^{(0)}(\mathbf{r}) = -4\pi \left[\frac{1}{L^3} \sum_{\mathbf{k}} e^{i\mathbf{k} \cdot \mathbf{r}} - \frac{1}{L^3} \right]. \quad (\text{S6})$$

It will be shown shortly that it is this $1/L^3$ contribution to the uniform background that gets distorted into a Gaussian charge distribution by SCA, while the ‘ λ contributions’ are unaffected. It is the latter that give rise to terms in the Hamiltonian proportional to $|\mathbf{M}|^2$ (see e.g. Ref. 78), such as when a constant electric displacement field is imposed.⁴⁸

Let us now consider a point charge q at the origin, along with a compensating Gaussian charge distribution, also centered at the origin:

$$n_{\text{SCA},0}(\mathbf{r}) = q\delta(\mathbf{r}) - q\kappa \exp(-\kappa^2 r^2)/\sqrt{\pi}. \quad (\text{S7})$$

The potential due to $n_{\text{SCA},0}$ is

$$\phi_0(\mathbf{r}) = \frac{q \operatorname{erfc}(\kappa|\mathbf{r}|)}{|\mathbf{r}|}. \quad (\text{S8})$$

Now consider the charge distribution to due a periodic array of $n_{\text{SCA},0}$,

$$n_{\text{SCA}}(\mathbf{r}) = \sum_{\mathbf{n}} n_{\text{SCA},0}(\mathbf{r} + \mathbf{n}L). \quad (\text{S9})$$

By linear superposition, this gives rise to a potential,

$$\phi(\mathbf{r}) = \sum_{\mathbf{n}} \frac{q \operatorname{erfc}(\kappa|\mathbf{r} + \mathbf{n}L|)}{|\mathbf{r} + \mathbf{n}L|}. \quad (\text{S10})$$

Now let us return to the Green’s function. In the main text, Eq. 5 was obtained by simply neglecting the sum in reciprocal space in Eq. 4. Considering the arguments above leading to Eq. S10 (setting $q = 1$), and from the uniqueness theorem of electrostatics,

$$\nabla^2 \psi_{\text{SCA}}^{(\lambda)}(\mathbf{r}) = -4\pi \left[n_{\text{SCA}}(\mathbf{r}) + \frac{\lambda}{L^3} \right]. \quad (\text{S11})$$

Thus $\psi_{\text{SCA}}^{(\lambda)}$ is the Green’s function for a periodically replicated unit point charge with a compensating Gaussian charge, *and* embedded in a uniform charge distribution λ/L^3 . Again, it is instructive to consider tin-foil boundary conditions explicitly,

$$\nabla^2 \psi_{\text{SCA}}^{(0)}(\mathbf{r}) = -4\pi n_{\text{SCA}}(\mathbf{r}). \quad (\text{S12})$$

Comparing Eqs. S6 and S12 makes it apparent that under tin-foil boundary conditions, SCA alters the charge distribution by distorting the compensating uniform background charge (associated with every point charge in the system) into a compensating Gaussian charge distribution.

NOTES ON THE DIELECTRIC CONSTANT FOR A SHORT-RANGED SYSTEM

The purpose of this section is to present a perspective on how the dielectric constant in a system with short-ranged electrostatic interactions can be understood. For simplicity, an infinite system is considered. To begin, consider the Maxwell equation for dielectrics, relating the electric displacement \mathbf{D} to the Maxwell electric field \mathbf{E} and polarization \mathbf{P} :

$$\mathbf{D}(\mathbf{r}) = \mathbf{E}(\mathbf{r}) + 4\pi\mathbf{P}(\mathbf{r}), \quad (\text{S13a})$$

$$\mathbf{D}(\mathbf{k}) = \mathbf{E}(\mathbf{k}) + 4\pi\mathbf{P}(\mathbf{k}). \quad (\text{S13b})$$

For convenience, the relation has been given both in real space (Eq. S13a) and reciprocal space (Eq. S13b). The dielectric tensor ϵ relates \mathbf{D} and \mathbf{E} ,

$$\mathbf{D}(\mathbf{r}) = \int d\mathbf{r}' \epsilon(\mathbf{r}, \mathbf{r}') \cdot \mathbf{E}(\mathbf{r}'), \quad (\text{S14a})$$

$$\mathbf{D}(\mathbf{k}) = \epsilon(\mathbf{k}) \cdot \mathbf{E}(\mathbf{k}). \quad (\text{S14b})$$

If one asserts that ϵ is unchanged irrespective of whether SCA or a full electrostatic treatment is used, then Eq. S14 suggests that one way to view any differences in dielectric screening as due to differences in \mathbf{E} (and consequently \mathbf{D}).

It is argued below that this viewpoint is useful for understanding the properties of the LMFT/SCA system presented in the main article.

It is useful to state some additional known results for the infinite system in which a full electrostatic treatment is used (see e.g. Ref. 45). Combining Eqs. S13b and S14b gives,

$$4\pi\mathbf{P}(\mathbf{k}) = [\boldsymbol{\epsilon}(\mathbf{k}) - \mathbf{1}] \cdot \mathbf{E}(\mathbf{k}) \equiv 4\pi\boldsymbol{\chi}(\mathbf{k}) \cdot \mathbf{E}(\mathbf{k}), \quad (\text{S15})$$

where $\mathbf{1}$ is the unit tensor. Both \mathbf{P} and \mathbf{E} depend upon the shape of the sample. In contrast, both $\boldsymbol{\epsilon}$ and $\boldsymbol{\chi}$ are shape-independent quantities. The polarization can also be expressed in terms of the external field $\mathbf{E}^{(0)}$,

$$4\pi\mathbf{P}(\mathbf{k}) = 4\pi\boldsymbol{\chi}^{(0)}(\mathbf{k}) \cdot \mathbf{E}^{(0)}(\mathbf{k}). \quad (\text{S16})$$

The external susceptibility $\boldsymbol{\chi}^{(0)}$ is of interest as it is directly related to molecular correlations in the system. As $\mathbf{E}^{(0)}$ is shape-independent, however, it immediately follows that $\boldsymbol{\chi}^{(0)}$ depends upon sample shape. Relating $\boldsymbol{\chi}^{(0)}$ to $\boldsymbol{\epsilon}$ is most readily achieved by relating \mathbf{E} to $\mathbf{E}^{(0)}$. For the infinite system considered here,

$$\mathbf{E}(\mathbf{k}) = \mathbf{E}^{(0)}(\mathbf{k}) - 4\pi\hat{\mathbf{k}}\hat{\mathbf{k}} \cdot \mathbf{P}(\mathbf{k}). \quad (\text{S17})$$

Combining Eqs. S15, S16 and S17 gives,

$$\boldsymbol{\chi}^{(0)}(\mathbf{k}) = [\mathbf{1} + 4\pi\hat{\mathbf{k}}\hat{\mathbf{k}} \cdot \boldsymbol{\chi}(\mathbf{k})]^{-1} \cdot \boldsymbol{\chi}(\mathbf{k}). \quad (\text{S18})$$

For an isotropic system, if $\boldsymbol{\epsilon}$ is an intensive property then it cannot depend upon the direction of \mathbf{k} . Thus,

$$\lim_{\mathbf{k} \rightarrow \mathbf{0}} \boldsymbol{\epsilon}(\mathbf{k}) = \epsilon \mathbf{1},$$

where ϵ is a scalar. This leads to the familiar results for the transverse (perpendicular to $\hat{\mathbf{k}}$) and longitudinal (parallel to $\hat{\mathbf{k}}$) components of $\boldsymbol{\chi}^{(0)}$:

$$\lim_{\mathbf{k} \rightarrow \mathbf{0}} 4\pi\chi_{xx}^{(0)}(\mathbf{k}) = \lim_{\mathbf{k} \rightarrow \mathbf{0}} 4\pi\chi_{yy}^{(0)}(\mathbf{k}) = \epsilon - 1, \quad (\text{S19a})$$

$$\lim_{\mathbf{k} \rightarrow \mathbf{0}} 4\pi\chi_{zz}^{(0)}(\mathbf{k}) = \frac{\epsilon - 1}{\epsilon}. \quad (\text{S19b})$$

Following convention, a coordinate system has been chosen such that $\hat{\mathbf{k}}$ defines the z direction.

For the SCA system, Eq. S17 now reads

$$\mathbf{E}(\mathbf{k}) = \mathbf{E}^{(0)}(\mathbf{k}) - 4\pi[1 - \exp(-k^2/4\kappa^2)]\hat{\mathbf{k}}\hat{\mathbf{k}} \cdot \mathbf{P}(\mathbf{k}). \quad (\text{S20})$$

It is apparent that, at long wavelengths, $\mathbf{E} \approx \mathbf{E}^{(0)}$, i.e. there is no depolarizing field in the SCA system. Similarly, Eq. S18 now reads

$$\boldsymbol{\chi}^{(0,\text{SCA})}(\mathbf{k}) = \left[\mathbf{1} + 4\pi[1 - \exp(-k^2/4\kappa^2)]\hat{\mathbf{k}}\hat{\mathbf{k}} \cdot \boldsymbol{\chi}(\mathbf{k}) \right]^{-1} \cdot \boldsymbol{\chi}(\mathbf{k}). \quad (\text{S21})$$

This leads to,

$$\lim_{\mathbf{k} \rightarrow \mathbf{0}} 4\pi\chi_{\alpha\alpha}^{(0,\text{SCA})}(\mathbf{k}) = \epsilon - 1, \quad (\text{S22})$$

with $\alpha = x, y$ or z . Taking ϵ to be unchanged between the full and SCA treatments for electrostatics, Eq. S22 appears in line with the results presented in the main paper (see Fig. 3 and Eq. 15).

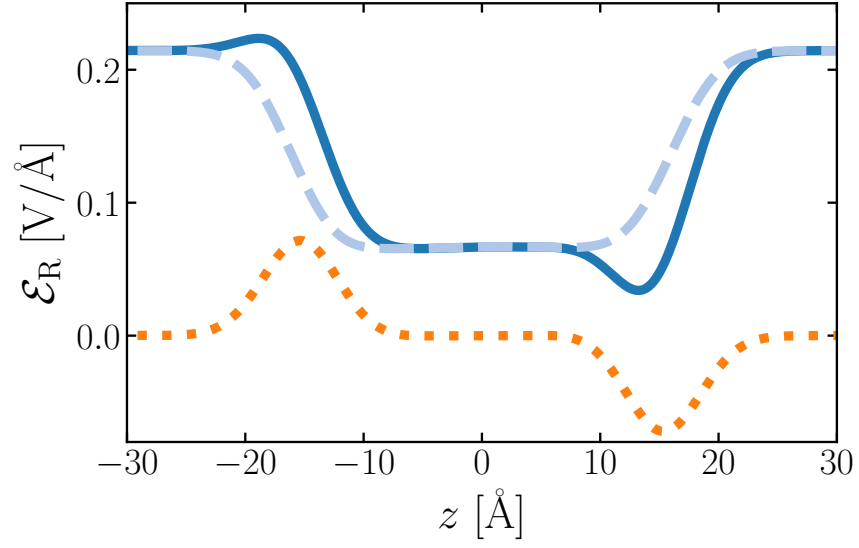


FIG. S1. Accounting for the effects of spontaneous charge density on the restructuring field. The dotted orange line shows \mathcal{E}_R for the confined water system with $D = 0 \text{ V/\AA}$, obtained from molecular simulation. The solid blue line shows \mathcal{E}_R with $D = 0.15 \text{ V/\AA}$, also obtained from molecular simulation. The dashed line results from subtracting the dotted orange line from the solid blue line (this is also presented in Fig. 4).